TITLE

TMEM16 and TMEM63/OSCA proteins share a conserved potential to permeate ions and phospholipids

AUTHORS

Augustus J. Lowry[1,†], Pengfei Liang[1,†], Y.C. Serena Wan[1], Zhen-Ming Pei[3], Huanghe Yang[1,2,*], Yang Zhang[1,4,†,*]

[1]Department of Biochemistry, Duke University School of Medicine, Durham, NC 27710, USA

[2]Department of Neurobiology, Duke University School of Medicine, Durham, NC 27710, USA

[3]Department of Biology, Duke University, Durham, NC 27710, USA

[4]Current address: Shenzhen Bay Laboratory, Guangdong 518106, China

[†]Denotes equal contribution

*To whom correspondence should be addressed

ABSTRACT

The calcium-activated TMEM16 proteins and the mechanosensitive/osmolarity-activated OSCA/TMEM63 proteins belong to the Transmembrane Channel/Scramblase (TCS) superfamily. Within the superfamily, OSCA/TMEM63 proteins, as well as TMEM16A and TMEM16B, likely function solely as ion channels. However, the remaining TMEM16 members, including TMEM16F, maintain an additional function as scramblases, rapidly exchanging phospholipids between leaflets of the membrane. Although recent studies have advanced our understanding of TCS structure-function relationships, the molecular determinants of TCS ion and lipid permeation remain unclear. Here we show that single lysine mutations in transmembrane helix (TM) 4 allow non-scrambling TCS members to permeate phospholipids. This study highlights the key role of TM 4 in controlling TCS ion and lipid permeation and offers novel insights into the evolution of the TCS superfamily, suggesting that, like TMEM16s, the OSCA/TMEM63 family maintains a conserved potential to permeate ions and phospholipids.

INTRODUCTION

Ion channels and phospholipid scramblases catalyze the passive flux of ions and phospholipids down their respective chemical gradients. Compared to ion channels, both our understanding of scramblases and the evolutionary origins of phospholipid scrambling are underdeveloped. Discoveries of two scramblase families—the TMEM16 calcium-activated phospholipid scramblases (CaPLSases) and XKR caspase-dependent phospholipid scramblases—have revealed roles for scramblases in processes such as blood coagulation[1], cell death signaling[2], phagocytosis[3], cell migration[4], membrane repair[5,6], microparticle release[7], cell-cell fusion[8–10], and viral infection[11,12]. Among identified scramblases, TMEM16 CaPLSases are the most extensively studied at the molecular level[13]. The TMEM16 family (Extended Data Fig. 1a) was originally classified as calcium-activated chloride channels (CaCCs) based on the first-discovered members, TMEM16A and TMEM16B[14–16]. The remaining members, however, exhibit CaPLSase activity, with TMEM16F representing the canonical CaPLSase[17] (Fig. 1a). Uniquely, CaPLSases also function as non-selective ion channels along with their non-specific permeability to phospholipids. Substrate permeation is facilitated by calcium-induced conformational changes causing the clamshell-like separation of TMs 4 and 6 to facilitate ion and phospholipid permeation[18–20] (Extended Data Fig. 1b-e). These conformational changes further catalyzed phospholipid permeation by thinning the membrane near the permeation pathway[21,22].

The TMEM16 family together with the TMEM63/OSCA family and TMC family[23–26] collectively form the Transmembrane Channel/Scramblase (TCS) superfamily[13]. Despite the conserved 10-TM architectural core[27–31], phospholipid permeability has not been experimentally demonstrated in mechanosensitive TMEM63/OSCA or TMC proteins, raising the intriguing question of how TCS proteins discriminate between ion and ion/phospholipid substrates. Interestingly, studies have shown that the TMEM16A CaCC can be genetically modified to enable phospholipid permeability, either by substituting TMEM16F domains as small as 15 amino acids[32], or through a single lysine mutation in TM 4 at the

51 hydrophobic gate[18]. These findings suggest a modest energetic barrier for scramblase activity and lead
52 us to hypothesize that evolutionary relatives of the TMEM16 family may maintain a conserved potential
53 for both ion and phospholipid permeation.

54 To test this hypothesis, we introduced single lysine mutations along TM 4 of TMEM16F,
55 TMEM16A, OSCA1.2, and TMEM63A at sites near the corresponding hydrophobic gate of TMEM16F[18].
56 TM 4 lysine mutations in TMEM16F and TMEM16A resulted in constitutive phospholipid scramblase
57 activity. Strikingly, the equivalent TM 4 lysine mutations of OSCA1.2 and TMEM63A also converted
58 these ion channels into phospholipid scramblases, which were either constitutively open or further
59 activated by osmotic stimulation. All mutants also resulted in commensurate gain-of-function ion
60 channel activity, suggesting that the charge in TM 4 disrupts the activation gate of these evolutionarily
61 related proteins. Together, our findings advance the mechanistic understanding of gating and substrate
62 permeation in the TMEM16 and OSCA/TMEM63 families, underscore a key design principle for
63 phospholipid scramblases, and support our hypothesis that the TCS superfamily maintains a conserved
64 potential for both ion and phospholipid permeation.

65 **RESULTS**

66 **TM 4 lysine mutations result in a constitutively active TMEM16F scramblase**

67 Our previous study identified the activation gate of TMEM16F, consisting of hydrophobic
68 residues from TMs 4, 5, and 6, which collectively govern ion and phospholipid permeation[18]. Introducing
69 polar or charged residues to the activation gate results in gain-of-function (GOF) CaPLSases, some of
70 which are constitutively activated without requiring calcium. Structural and computational studies on
71 the fungal *Nh*TMEM16[33] and *Af*TMEM16[21] orthologs, as well as human TMEM16K[34] further support a
72 clamshell like gating model[18] whereby scrambling activity is promoted by separation of the TM 4/6
73 interface[13] (Extended Data Fig. 1b-d). The conformational transition involves the N-terminal half of TM
74 4, which bends away from TM 6, and the C-terminal half of TM 6, which collapses onto the calcium

75 binding sites formed together with TMs 7 and 8[13]. Given that the N-termini of TM 4 are largely
76 hydrophobic among TMEM16 CaPLSases (Extended Data Fig. 1f) and a lysine mutation at F518 leads
77 to a constitutively open TMEM16F activation gate[18], we hypothesized that introducing a charged side
78 chain along the TM 4/6 interface might disrupt the hydrophobic gate and result in TMEM16 scramblases
79 with GOF scramblase activity. To test this hypothesis, we overexpressed eGFP-tagged mutant
80 constructs in TMEM16F knockout (KO) HEK293T cells and used an established scramblase
81 assay[18,35,36] that detects phosphatidylserine (PS) exposure using fluorophore-tagged Annexin V (AnV)
82 as a reporter (Fig. 1b). In the absence of calcium stimulation, PS is predominantly in the inner leaflet of
83 the plasma membrane of the TMEM16F wildtype (WT) expressing cells and is therefore not labelled by
84 extracellular AnV. Similar to TMEM16F F518K[18], overexpressing the single lysine mutations TMEM16F
85 I521K and M522K led to spontaneous, global exposure of PS on the plasma membrane without
86 requiring calcium stimulation (Fig. 1b, c). We further tested whether I521K and M522K have GOF ion
87 channel activity using whole-cell patch clamp. In the absence of calcium, the mutants, but not WT
88 TMEM16F, showed robust depolarization-activated outward rectifying currents (Fig. 1d-f). Our imaging
89 and patch clamp experiments thus demonstrate that I521K and M522K are functionally expressed on
90 the plasma membrane and their GOF lipid scramblase activity results in spontaneous, global PS
91 exposure on the cell surface. I521 and M522 are approximately one helical turn below the hydrophobic
92 gate residue, F518,[18] (Fig. 1a) supporting the idea that a lysine mutation on TM 4 along the TM 4/6
93 interface promotes gate opening and substrate permeation (Fig. 1g).

94 **TM 4 lysine mutations convert TMEM16A into a constitutively active scramblase**

95 TMEM16A is a CaCC[14–16] without scramblase activity (Fig. 2a-c)[18,32]. We previously reported
96 that a single TM 4 lysine mutation (L543K) at the hydrophobic gate of TMEM16A (Fig. 2a) allows the
97 CaCC to permeate phospholipids spontaneously, analogous to the F518K mutation in TMEM16F[18].
98 Thus, we reasoned that lysine mutations equivalent to TMEM16F I521K and M522K might also result

99 in spontaneous phospholipid permeability. To test this hypothesis, we overexpressed eGFP-tagged
100 TMEM16A I546K and I547K mutants in TMEM16F KO HEK293T cells, and assessed their ability to
101 expose PS on the plasma membrane with confocal microscopy. Similar to TMEM16A L543K[18], I546K-
102 and I547K-expressing cells exhibit spontaneous, global PS exposure (Fig. 2b, c), analogous to the
103 equivalent TMEM16F mutations I521K and M522K (Extended Data Fig. 1f; Fig. 1b, c). Similarly, whole-
104 cell patch clamp revealed GOF ion channel activity at depolarizing potentials, even in the absence of
105 calcium stimulation (Fig. 2d-f). Together, these results suggest that lysine mutations in this region
106 strongly destabilize the hydrophobic gate to endow the TMEM16A CaCC with constitutive phospholipid
107 permeability and GOF ion channel activity (Fig. 2g).

108 **TM 4 lysine mutation L438K converts OSCA1.2 into a constitutively active scramblase**

109 We next applied our approach to a TMEM16 relative from the OSCA/TMEM63 family (Extended Data
110 Fig. 1a), which was first discovered in plants as a family of mechanosensitive and osmolarity-activated
111 cation non-selective ion channels[37] (Fig. 3a). We hypothesized that analogous lysine mutations on TM
112 4 along the TM 4/6 interface of OSCA/TMEM63 proteins would result in GOF channels that may also
113 permeate phospholipids. Within the family, we chose OSCA1.2 from *Arabidopsis thaliana* due to
114 previous structural[27] and biophysical[38] characterization demonstrating that the channel is activated
115 directly by membrane tension. Overexpressing eGFP-tagged OSCA1.2 WT in TMEM16F KO HEK293T
116 cells did not induce PS exposure, demonstrating that OSCA1.2 WT lacks spontaneous lipid scrambling
117 activity (Fig. 3b). We then introduced TM 4 lysine mutations near the putative gating residues identified
118 by structural (Fig. 3a) and sequence alignment (Extended Data Fig. 1e). Strikingly, a single point
119 mutation, L438K, causes cells overexpressing the OSCA1.2 mutant to exhibit spontaneous and global
120 PS exposure (Fig. 3b, c). This mirrors our results with both TMEM16F (Fig. 1) and TMEM16A (Fig. 2),
121 suggesting that the L438K mutation allows the OSCA1.2 channel to permeate phospholipids. Next, we
122 used inside-out patch clamp to examine if L438K also enhances OSCA1.2 channel activity. We found

123 that the mutant significantly left-shifts the conductance-voltage (*G-V*) relationship (Fig. 3e, f) and
124 accelerates channel activation kinetics (Fig. 3g) compared to WT. Under -50 mmHg of pressure, L438K
125 has half-maximal voltages ($V_{0.5}$) of 66.7±3.7 mV, while the WT $V_{0.5}$ is nearly 108.7±5.6 mV (Fig. 3f),
126 underscoring that this mutation also disrupts channel gating. Together, these experiments show that,
127 like TMEM16A, a single lysine mutation near the putative gate allows the mechanosensitive and
128 osmolarity-activated OSCA1.2 channel to become spontaneously permeable to phospholipids (Fig. 3h).

129 **TM 4 lysine mutation A439K converts OSCA1.2 into an osmolarity-sensing scramblase**

130 Interestingly, mutating the neighboring amino acid (Fig. 3a), A439, to lysine resulted in minimal
131 spontaneous PS exposure (Fig. 3b, c). We thus reasoned that A439K scramblase activity may require
132 additional stimulation. Given that OSCA1.2 is an osmolarity-sensitive ion channel[38] and reduction of
133 extracellular osmolarity does not induce PS exposure in OSCA1.2 WT expressing cells (Fig. 4a, c), we
134 acutely treated A439K-expressing cells with a hypotonic solution (120 mOsm/kg). Indeed, PS exposure
135 was robustly induced (Fig. 4b, c). Inside-out patch clamp further demonstrated that A439K enhances
136 OSCA1.2 ion channel activity as evidenced by the accelerated activation kinetics (Fig. 3g) and left-
137 shifted *G-V* relationship (Fig. 3f). Our experiments thus indicate that A439K disrupts OSCA1.2 gating
138 and converts the osmolarity-activated ion channel into an osmolarity-activated phospholipid scramblase
139 (Fig. 4d).

140 **TM 4 lysine mutations convert TMEM63A into a constitutively active scramblase**

141 We next turned our attention to TMEM63A to further investigate the evolutionary conservation
142 of our observation that TM 4 lysine mutations convert TMEM16 and OSCA members into scramblases.
143 TMEM63s represent the mammalian members of the OSCA/TMEM63 family with three members
144 present in humans (TMEM63A-C). Recent structural and functional characterizations indicate that
145 TMEM63s function as mechanosensitive ion channels gated by high-threshold membrane tension and,
146 in notable contrast to all other structurally resolved TCS members, they likely function as monomers[39–

147 [41]. Given their structural homology to TMEM16s and OSCA1.2[39], we hypothesized that TM 4 mutations
148 in TMEM63A would also result in GOF activity. We again identified residues near the putative gate by
149 structural (Fig. 5a) and sequence alignment (Extended Data Fig. 1f), selecting W472 (equivalent to
150 F518 in TMEM16F and L543 in TMEM16A) and S475 (equivalent to L438 in OSCA1.2). Indeed,
151 overexpressing eGFP-tagged mouse TMEM63A with single lysine mutations at either W472 and S475
152 led to spontaneous PS exposure (Fig. 5b, c), though the AnV staining revealed punctate rather than
153 global patterns of PS exposure. To confirm membrane localization and further probe mutant effects,
154 we exploited TMEM63A ion channel function using cell-attached patch clamp. As TMEM63A exhibits
155 voltage-dependent activity under high pressures, we compared mutant and WT *I-V* relationships at -80
156 mmHg. W472K and S475K caused marked reductions in $V_{0.5}$ from 122.3±3.5 mV for WT to 95.9±6.3
157 mV and 92.1±8.6 mV, respectively (Fig. 5d-f). Together, these results are consistent with our
158 observations in TMEM16F, TMEM16A, and OSCA1.2, indicating that single lysine mutations along TM
159 4 of TMEM63A can facilitate both ion and phospholipid permeation (Fig. 5g).

160 **DISCUSSION**

161 Mechanistically, our study improves models of TMEM16 substrate permeation and gating. We
162 identified multiple lysine mutations in TMEM16F and TMEM16A that promote phospholipid permeation
163 and cause commensurate changes in ion channel activities. Our findings complement functional
164 characterizations of TMEM16F gating mutants where gate destabilization is inversely correlated with
165 side chain hydropathy[18,42]. Lysine is above only arginine on the hydropathy index and thus likely
166 explains why it readily destabilizes the gate. For instance, F518K exhibits spontaneous PS exposure,
167 even when the calcium binding site is destroyed[18], whereas F518H does not exhibit spontaneous PS
168 exposure[42]. Interestingly, the recent TMEM16F F518H structure (Extended Data Fig. 1d) shows local
169 membrane thinning due in part to unexpected conformational changes in TM 3[42]. Future structural
170 studies are needed to assess whether TMEM16A or OSCA/TMEM63 mutant scramblases also promote

171 membrane thinning and/or conformational rearrangements in TM 3. More broadly, our results highlight
172 an increasingly appreciated design principle of scramblases where polar and charged residues often
173 line a membrane-spanning groove. This observation has been noted for TMEM16[43,34,44], Xkr[45,46], and
174 opsin[47] scramblases and should be a key criterion for identifying and characterizing new scramblases.
175 Our findings also advance our understanding of evolutionary relatives of the TCS superfamily[13]
176 and help uncover their roles in human diseases. Although OSCA/TMEM63 proteins are not known to
177 scramble phospholipids, we show that TM 4 lysine mutations in OSCA1.2 and TMEM63A convert these
178 osmolarity-activated and mechanosensitive ion channels into phospholipid scramblases, analogous to
179 our findings with the equivalent TMEM16A mutations. We thus speculate that the conserved structural
180 architecture in the transmembrane region endows TCS proteins with a potential to scramble
181 phospholipids, though this capability may have been lost during evolution. It will be interesting to test
182 whether equivalent TM 4 lysine mutations can convert transmembrane channel-like (TMC) proteins—
183 the third TCS relative of TMEM16 and OSCA/TMEM63[13]—into phospholipid scramblases. TMC1 and
184 TMC2 are best known for their roles in auditory sensation, and thus far have mostly been characterized
185 *in vivo* due to expression difficulties in heterologous systems[48]. However, recent *in vivo* characterization
186 of mouse TMC1 M412K, known as the *Beethoven* mutation, provided an important insight[49]. The
187 deafness-associated mutation is located in TM 4 (Extended Data Fig. 1f; equivalent of M522 in
188 TMEM16F, I547 in TMEM16A, and A439 in OSCA1.2) and results in constitutive PS exposure when
189 expressed in the hair cell membranes of both heterozygous and homozygous mice[49]. This raises the
190 intriguing possibility that the *Beethoven* mutation may enable TMC1 to spontaneously permeate
191 phospholipids, leading to a loss of membrane homeostasis and ultimately, auditory sensation[50]. The
192 possibility of converting TMC proteins into phospholipid scramblases should be thoroughly investigated.
193 Additionally, disease-associated mutations in TMEM63 proteins are present along the TM 4/6 interface,
194 such as TMEM63B T481N[49]. We speculate that introducing more hydropathic side chains along this

interface may lead to spontaneous ion and or phospholipid permeability, perhaps contributing to underlying pathophysiology.

METHODS

Cloning and mutagenesis

All constructs use a peGFP-N1 vector backbone. Wild type sequence and mutation numbers correspond to NCBI: NP_780553.2 (*Mus musculus* TMEM16F) with a three amino acid (MQM) N-terminal truncation, NCBI: NP_001229278 (*Mus musculus* TMEM16A), GenBank: AIU34614.1 (*Arabidopsis thaliana* OSCA1.2), and NCBI: NP_001404481.1 (*Mus musculus* TMEM63A). *At*OSCA1.2 and *Mm*TMEM63A cDNAs were subcloned using In-Fusion Snap Assembly (Takara, #638947). Point mutants were generated by PCR site-directed mutagenesis with primers from IDT DNA Technologies. Sequences were confirmed by Sanger sequencing (Azenta).

Bioinformatics

The following sequences were obtained from UniProt and aligned using Clustal Omega: Q8BHY3-2 (*Mm*TMEM16A), Q9NQ90 (*Hs*TMEM16B), Q9BYT9 (*Hs*TMEM16C), Q32M45 (*Hs*TMEM16D), Q75V66 (*Hs*TMEM16E), Q6P9J9 (*Mm*TMEM16F), Q6IWH7 (*Hs*TMEM16G), Q9HCE9 (*Hs*TMEM16H), A1A5B4 (*Hs*TMEM16J), Q9NW15 (*Hs*TMEM16K), C7Z7K1 (*Nh*TMEM16), Q4WA18 (*Af*TMEM16), Q9XEA1 (*At*OSCA1.1), Q5XEZ5 (*At*OSC1.2), B5TYT3 (*At*OSCA1.3), A0A097NUQ0 (*At*OSCA1.4), A0A097NUS0 (*At*OSCA1.5), A0A097NUP1 (*At*OSCA1.6), A0A097NUP8 (*At*OSCA1.7), A0A097NUQ2 (*At*OSCA1.8), A0A097NUQ5 (*At*OSCA2.1), A0A097NUS5 (*At*OSCA2.2), A0A097NUP6 (*At*OSCA2.3), A0A097NUQ3 (*At*OSCA2.4), A0A097NUQ7 (*At*OSCA2.5), Q9C8G5 (*At*OSCA3.1), A0A097NUT0 (*At*OSCA4.1), Q91YT8 (*Mm*TMEM63A), Q5T3F8 (*Hs*TMEM63B), and Q9P1W3 (*Hs*TMEM63C), Q8R4P5 (*Mm*TMC1), Q8R4P4 (*Mm*TMC2), Q7TQ69 (*Mm*TMC3), Q7TQ65 (*Mm*TMC4), Q32NZ6 (*Mm*TMC5), Q7TN60 (*Mm*TMC6), Q8C428 (*Mm*TMC7), and Q7TN58 (*Mm*TMC8). A subset of the

218 alignment was selected for Extended Data Fig. 1. Structural models were obtained from the PDB,
219 aligned, and visualized using Pymol (Schrödinger).

220 ***Cell culture***

221 The HEK293T cell line was authenticated by the Duke Cell Culture Facility. The TMEM16F KO
222 HEK293T cell line was generated by the Duke Functional Genomics Core and characterized in previous
223 studies[18,35]. All cells were cultured with DMEM (Gibco, #11995-065) supplemented with 10% fetal
224 bovine serum (FBS) (Sigma-Aldrich, # F2442) and 1% penicillin/streptomycin (Gibco, #15-140-122) at
225 37°C in 5% CO_2-95% air.

226 ***Transfection***

227 Plasmids were transiently transfected into TMEM16F KO HEK 293T cells by using X-tremeGENE9 or
228 X-tremeGENE360 transfection reagents (MilliporeSigma). Media was replaced with calcium free DMEM
229 (Gibco, 21068-028) 3-4 hours after transfection. The transfected cells were imaged or patched 18-24
230 or 18-48 hours after transfection, respectively.

231 ***Fluorescence imaging of scramblase-mediated PS Exposure***

232 A Zeiss 780 inverted confocal microscope was used to monitor scramblase activity in live cells using
233 the methods described in previous publications[9,18,35]. Briefly, 18-24 hours after transfection, the cells
234 were incubated in AnV buffer (1:175 dilution of the fluorescently tagged AnV (Biotium) in Hank's
235 balanced salt solution) before imaging. Spontaneous PS positive cells were labeled by fluorescently
236 tagged AnV and imaged. Results were quantified as a percentage of PS positive cells among all GFP
237 positive cells. For osmolarity activation, 2 mM $CaCl_2$ in ddH_2O was added to the AnV buffer at a 2:1
238 ratio. The final osmolarity was ~120 mOsm/kg as measured by a micro-osmometer (Advanced
239 Instrument). Cells overexpressing WT or mutant OSCA1.2 were treated with low osmolarity AnV buffer,
240 and the scramblase activity was measured by recording fluorescent AnV surface accumulation at 5

241 second intervals. A custom MATLAB code was used to quantify AnV signal and is available at Github
242 (https://github.com/yanghuanghe/scrambling_activity).

243 ***Electrophysiology***

244 All electrophysiology recordings were conducted using an Axopatch 200B amplifier with the signal
245 digitally sampled at 10 kHz using an Axon Digidata 1550A (Molecular Devices, Inc.). All
246 electrophysiology recordings were carried out at room temperature 18-48 hours after transfection.
247 Glass pipettes were pulled from borosilicate capillaries (Sutter Instruments) and fire-polished using a
248 microforge (Narishige). Pipettes had resistances of 2–3 MΩ in bath solution.

249 ***Inside-out patch clamp recordings.*** The pipette solution (external) contained 140 mM NaCl,
250 10 mM HEPES, 2 mM $MgCl_2$, adjusted to pH 7.3 (NaOH), and the bath solution (internal) contained
251 140 mM NaCl, 10 mM HEPES, 5 mM EGTA, adjusted to pH 7.3 (NaOH). OSCA1.2 WT and mutations
252 were held at constant pressure administrated using a syringe calibrated with a manometer, similar to a
253 previous study[54]. Patches were held at a membrane potential of -60 mV and at the indicated pressure,
254 then stimulated using the indicated voltage protocol.

255 ***Cell-attached patch clamp recordings.*** For TMEM63 recordings, cell-attach mode was used.
256 The bath solution contained (in mM): 140 KCl, 10 HEPES, 2 $MgCl_2$, 10 glucose, pH 7.3 adjusted with
257 KOH. The pipette solution contained (in mM): 130 NaCl, 5 KCl, 10 HEPES, 10 TEA-Cl, 1 $CaCl_2$, 1
258 $MgCl_2$, pH 7.3 (with NaOH). The mechano-activated current was evoked with a 200 ms pressure pulse
259 at -80 mmHg using a high-speed pressure clamp system (HSPC-1, ALA Scientific Instruments,
260 Farmingdale, NY). The membrane potential inside the patch was held at -60 mV. The voltage pulse
261 alone was run first followed by voltage pulse with pressure. The mechanosensitive current was obtained
262 by subtracting the voltage pulse from the voltage with pressure pulse.

263 ***Whole cell patch clamp recordings.*** The pipette solution (internal) contained 140 mM CsCl,
264 10 mM HEPES, 5 mM EGTA, adjusted to pH 7.3 (CsOH), and the bath solution (external) contained

140 mM NaCl, 10 mM HEPES, 5 mM EGTA, adjusted to pH 7.3 (NaOH). Patches were held at a membrane potential of -60 mV, then stimulated using the indicated voltage protocol.

Data analysis for electrophysiology

All data analysis was performed using Clampfit (Molecular Devices), Excel (Microsoft), MATLAB (MathWorks), and Prism softwares (GraphPad). Individual *G-V* curves were fitted with a Boltzmann function,

$$G = \frac{G_{max}}{1+e^{\frac{-ZF(V-V_{0.5})}{RT}}} \qquad (2)$$

where G_{max} denotes the fitted value for maximal conductance, $V_{0.5}$ denotes the voltage of half maximal activation of conductance, Z denotes the net charge moved across the membrane during the transition from the closed to the open state, and F denotes the Faraday constant.

REFERENCES

1. Suzuki, J., Umeda, M., Sims, P. J. & Nagata, S. Calcium-dependent phospholipid scrambling by TMEM16F. *Nature* **468**, 834–838 (2010).
2. Suzuki, J., Denning, D. P., Imanishi, E., Horvitz, H. R. & Nagata, S. Xk-related protein 8 and CED-8 promote phosphatidylserine exposure in apoptotic cells. *Science* **341**, 403–406 (2013).
3. Fadok, V. A. *et al.* Exposure of phosphatidylserine on the surface of apoptotic lymphocytes triggers specific recognition and removal by macrophages. *J. Immunol.* **148**, 2207–2216 (1992).
4. Chang, Z. *et al.* Anoctamin5 regulates cell migration and invasion in thyroid cancer. *Int. J. Oncol.* **51**, 1311–1319 (2017).
5. Griffin, D. A. *et al.* Defective membrane fusion and repair in Anoctamin5-deficient muscular dystrophy. *Hum. Mol. Genet.* **25**, 1900–1911 (2016).
6. Chandra, G. *et al.* Dysregulated calcium homeostasis prevents plasma membrane repair in Anoctamin 5/TMEM16E-deficient patient muscle cells. *Cell Death Discov.* **5**, 118 (2019).

288 7. Fujii, T., Sakata, A., Nishimura, S., Eto, K. & Nagata, S. TMEM16F is required for phosphatidylserine
289 exposure and microparticle release in activated mouse platelets. *Proc. Natl. Acad. Sci. U. S. A.* **112**,
290 12800–12805 (2015).
291 8. Whitlock, J. M., Yu, K., Cui, Y. Y. & Hartzell, H. C. Anoctamin 5/TMEM16E facilitates muscle
292 precursor cell fusion. *J. Gen. Physiol.* **150**, 1498–1509 (2018).
293 9. Zhang, Y. *et al.* TMEM16F phospholipid scramblase mediates trophoblast fusion and placental
294 development. *Sci. Adv.* **6**, eaba0310 (2020).
295 10. Zhang, Y. *et al.* Functional coupling between TRPV4 channel and TMEM16F modulates human
296 trophoblast fusion. *eLife* **11**, e78840 (2022).
297 11. Zaitseva, E. *et al.* Fusion Stage of HIV-1 Entry Depends on Virus-Induced Cell Surface Exposure
298 of Phosphatidylserine. *Cell Host Microbe* **22**, 99-110.e7 (2017).
299 12. Nanbo, A. *et al.* Ebola virus requires a host scramblase for externalization of phosphatidylserine
300 on the surface of viral particles. *PLoS Pathog.* **14**, e1006848 (2018).
301 13. Le, S. C., Liang, P., Lowry, A. J. & Yang, H. Gating and Regulatory Mechanisms of TMEM16 Ion
302 Channels and Scramblases. *Front. Physiol.* **12**, 787773 (2021).
303 14. Caputo, A. *et al.* TMEM16A, a membrane protein associated with calcium-dependent chloride
304 channel activity. *Science* **322**, 590–594 (2008).
305 15. Yang, Y. D. *et al.* TMEM16A confers receptor-activated calcium-dependent chloride
306 conductance. *Nature* **455**, 1210–1215 (2008).
307 16. Schroeder, B. C., Cheng, T., Jan, Y. N. & Jan, L. Y. Expression cloning of TMEM16A as a
308 calcium-activated chloride channel subunit. *Cell* **134**, 1019–1029 (2008).
309 17. Suzuki, J. *et al.* Calcium-dependent phospholipid scramblase activity of TMEM16 protein family
310 members. *J. Biol. Chem.* **288**, 13305–13316 (2013).

311 18. Le, T. *et al.* An inner activation gate controls TMEM16F phospholipid scrambling. *Nat. Commun.*
312 **10**, 1846 (2019).
313 19. Lam, A. K. M., Rheinberger, J., Paulino, C. & Dutzler, R. Gating the pore of the calcium-activated
314 chloride channel TMEM16A. *Nat. Commun.* **12**, 785 (2021).
315 20. Lam, A. K. M. & Dutzler, R. Mechanism of pore opening in the calcium-activated chloride channel
316 TMEM16A. *Nat. Commun.* **12**, 786 (2021).
317 21. Falzone, M. E. *et al.* Structural basis of Ca2+-dependent activation and lipid transport by a
318 TMEM16 scramblase. *eLife* **8**, e43229 (2019).
319 22. Falzone, M. E. *et al.* TMEM16 scramblases thin the membrane to enable lipid scrambling. *Nat.*
320 *Commun.* **13**, 2604 (2022).
321 23. Keresztes, G., Mutai, H. & Heller, S. TMC and EVER genes belong to a larger novel family, the
322 TMC gene family encoding transmembrane proteins. *BMC Genomics* **4**, 24 (2003).
323 24. Hahn, Y., Kim, D. S., Pastan, I. H. & Lee, B. Anoctamin and transmembrane channel-like
324 proteins are evolutionarily related. *Int. J. Mol. Med.* **24**, 51–55 (2009).
325 25. Medrano-Soto, A. *et al.* Bioinformatic characterization of the Anoctamin Superfamily of Ca2+-
326 activated ion channels and lipid scramblases. *PLOS ONE* **13**, e0192851 (2018).
327 26. Ballesteros, A., Fenollar-Ferrer, C. & Swartz, K. J. Structural relationship between the putative
328 hair cell mechanotransduction channel TMC1 and TMEM16 proteins. *eLife* **7**, e38433 (2018).
329 27. Jojoa-Cruz, S. *et al.* Cryo-EM structure of the mechanically activated ion channel OSCA1.2.
330 *eLife* **7**, e41845 (2018).
331 28. Liu, X., Wang, J. & Sun, L. Structure of the hyperosmolality-gated calcium-permeable channel
332 OSCA1.2. *Nat. Commun.* **9**, 5060 (2018).
333 29. Zhang, M. *et al.* Structure of the mechanosensitive OSCA channels. *Nat. Struct. Mol. Biol.* **25**,
334 850–858 (2018).

335 30. Maity, K. *et al.* Cryo-EM structure of OSCA1.2 from Oryza sativa elucidates the mechanical basis
336 of potential membrane hyperosmolality gating. *Proc. Natl. Acad. Sci. U. S. A.* **116**, 14309–14318
337 (2019).
338 31. Jeong, H. *et al.* Structures of the TMC-1 complex illuminate mechanosensory transduction.
339 *Nature* **610**, 796–803 (2022).
340 32. Yu, K. *et al.* Identification of a lipid scrambling domain in ANO6/TMEM16F. *eLife* **4**, e06901
341 (2015).
342 33. Kalienkova, V. *et al.* Stepwise activation mechanism of the scramblase nhTMEM16 revealed by
343 cryo-EM. *eLife* **8**, e44364 (2019).
344 34. Bushell, S. R. *et al.* The structural basis of lipid scrambling and inactivation in the endoplasmic
345 reticulum scramblase TMEM16K. *Nat. Commun.* **10**, 3956 (2019).
346 35. Le, T., Le, S. C. & Yang, H. Drosophila Subdued is a moonlighting transmembrane protein 16
347 (TMEM16) that transports ions and phospholipids. *J. Biol. Chem.* **294**, 4529–4537 (2019).
348 36. Le, T., Le, S. C., Zhang, Y., Liang, P. & Yang, H. Evidence that polyphenols do not inhibit the
349 phospholipid scramblase TMEM16F. *J. Biol. Chem.* **295**, 12537–12544 (2020).
350 37. Yuan, F. *et al.* OSCA1 mediates osmotic-stress-evoked Ca2+ increases vital for osmosensing
351 in Arabidopsis. *Nature* **514**, 367–371 (2014).
352 38. Murthy, S. E. *et al.* OSCA/TMEM63 are an Evolutionarily Conserved Family of Mechanically
353 Activated Ion Channels. *eLife* **7**, e41844 (2018).
354 39. Zheng, W. *et al.* TMEM63 proteins function as monomeric high-threshold mechanosensitive ion
355 channels. *Neuron* (2023) doi:10.1016/j.neuron.2023.07.006.
356 40. Qin, Y. *et al.* Cryo-EM structure of TMEM63C suggests it functions as a monomer. *Nat.*
357 *Commun.* **14**, 7265 (2023).

358 41. Wu, X., Shang, T., Lü, X., Luo, D. & Yang, D. A monomeric structure of human TMEM63A
359 protein. *Proteins* (2024) doi:10.1002/prot.26660.
360 42. Arndt, M. *et al.* Structural basis for the activation of the lipid scramblase TMEM16F. *Nat.*
361 *Commun.* **13**, 6692 (2022).
362 43. Brunner, J. D., Lim, N. K., Schenck, S., Duerst, A. & Dutzler, R. X-ray structure of a calcium-
363 activated TMEM16 lipid scramblase. *Nature* **516**, 207–212 (2014).
364 44. Alvadia, C. *et al.* Cryo-EM structures and functional characterization of the murine lipid
365 scramblase TMEM16F. *eLife* **8**, e44365 (2019).
366 45. Straub, M. S., Alvadia, C., Sawicka, M. & Dutzler, R. Cryo-EM structures of the caspase-
367 activated protein XKR9 involved in apoptotic lipid scrambling. *eLife* **10**, e69800 (2021).
368 46. Sakuragi, T. *et al.* The tertiary structure of the human Xkr8-Basigin complex that scrambles
369 phospholipids at plasma membranes. *Nat. Struct. Mol. Biol.* **28**, 825–834 (2021).
370 47. Morra, G. *et al.* Mechanisms of Lipid Scrambling by the G Protein-Coupled Receptor Opsin.
371 *Struct. Lond. Engl. 1993* **26**, 356-367.e3 (2018).
372 48. Pan, B. *et al.* TMC1 Forms the Pore of Mechanosensory Transduction Channels in Vertebrate
373 Inner Ear Hair Cells. *Neuron* **99**, 736-753.e6 (2018).
374 49. Ballesteros, A. & Swartz, K. J. Regulation of membrane homeostasis by TMC1
375 mechanoelectrical transduction channels is essential for hearing. *Sci. Adv.* **8**, eabm5550 (2022).
376 50. Sakuragi, T. & Nagata, S. Regulation of phospholipid distribution in the lipid bilayer by flippases
377 and scramblases. *Nat. Rev. Mol. Cell Biol.* 1–21 (2023) doi:10.1038/s41580-023-00604-z.
378 51. Kumar, S., Stecher, G., Li, M., Knyaz, C. & Tamura, K. MEGA X: Molecular Evolutionary
379 Genetics Analysis across Computing Platforms. *Mol. Biol. Evol.* **35**, 1547–1549 (2018).
380 52. Le, S. C., Jia, Z., Chen, J. & Yang, H. Molecular basis of PIP2-dependent regulation of the Ca2+-
381 activated chloride channel TMEM16A. *Nat. Commun.* **10**, 3769 (2019).

382 53. Liang, P. & Yang, H. Molecular underpinning of intracellular pH regulation on TMEM16F. *J. Gen.*
383 *Physiol.* **153**, e202012704 (2021).
384 54. Tsuchiya, M. *et al.* Cell surface flip-flop of phosphatidylserine is critical for PIEZO1-mediated
385 myotube formation. *Nat. Commun.* **9**, 2049 (2018).

386 **ACKNOWLEDGEMENTS**

387 This work was supported by the National Institute of Health (DP2GM126898 and R21GM146152 to
388 H.Y.) and the National Science Foundation Graduate Research Fellowship Program (DGE 2139754 to
389 A.J.L.). Any opinions, findings, and conclusions or recommendations expressed in this material are
390 those of the author(s) and do not necessarily reflect the views of the National Science Foundation.

391 **AUTHOR CONTRIBUTIONS**

392 H.Y. and Y.Z. conceived and H.Y. supervised the project. Y.Z. and A.J.L. imaging. P.L.
393 electrophysiology. A.J.L. sequence and structure alignments. A.J.L. and Y.C.S.W. cloning and
394 mutagenesis. Z.P. plasmids. Y.Z. MATLAB codes. A.J.L. and H.Y. drafted the manuscript with input
395 from all authors.

396 **COMPETING INTERESTS**

397 The authors declare no competing interests.

398

FIGURES

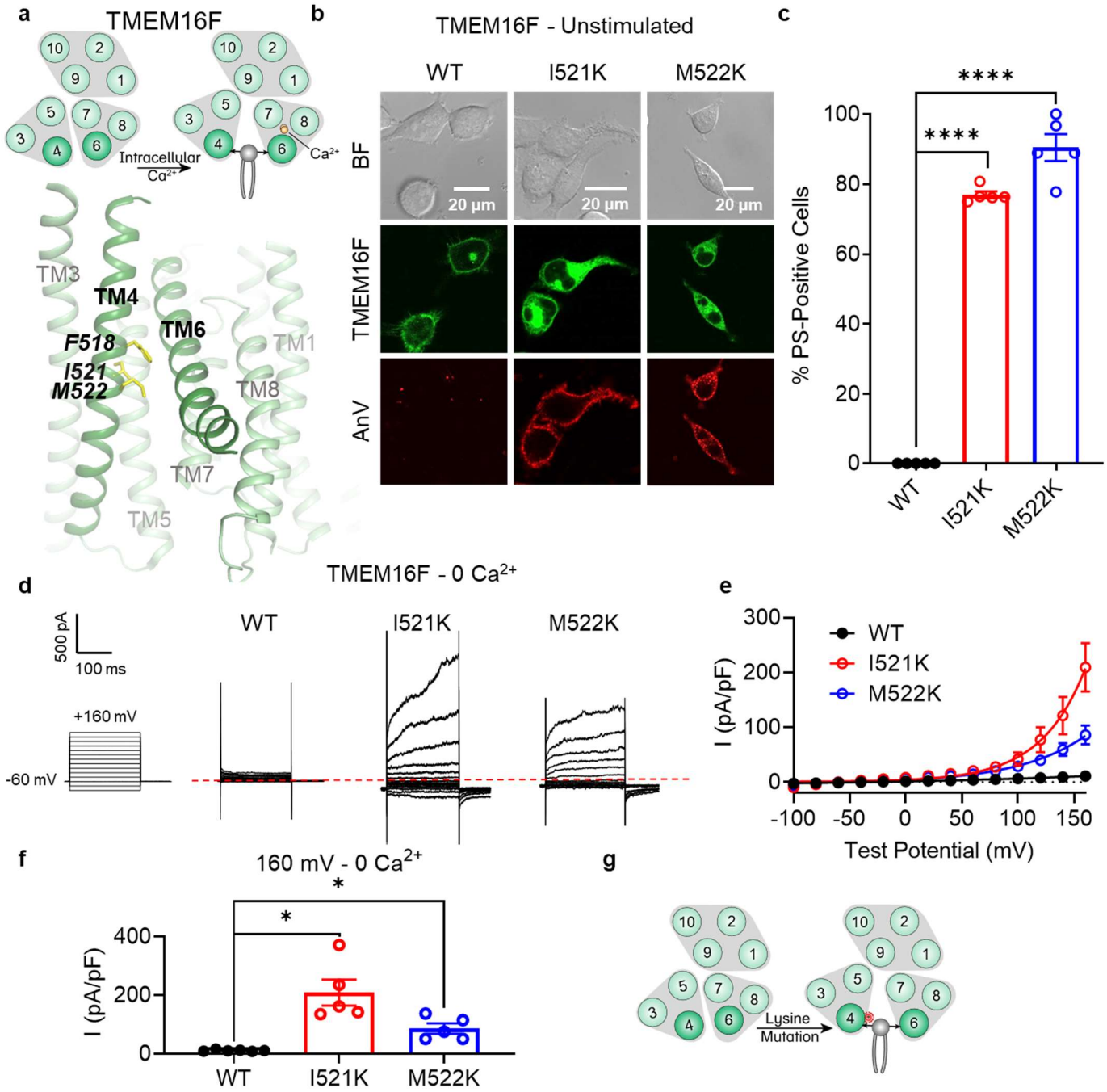

Figure 1: Lysine mutations along TM 4 enable TMEM16F channel and scramblase activities in the absence of calcium stimulation. (**a**) Top: TMEM16F is a calcium-activated phospholipid scramblase. Bottom: TM 4 mutant locations mapped on TMEM16F CaPLSase structure (PDB 6QPB). (**b**) Representative images of TMEM16F knockout (KO) HEK293T cells expressing eGFP-tagged

405 TMEM16F wildtype (WT), I521K, and M522K (center row). CF 594-conjugated Annexin V (AnV, bottom
406 row) labelled PS exposing cells. BF denotes bright field images (top row). (**c**) Quantification of the
407 percentage of cells with AnV labelling for TMEM16F WT (n=5), I521K (n=5), and M522K (n=5)
408 transfected cells. Values were derived from images of biological replicates, with error bars representing
409 standard error of the mean (SEM). Statistical comparisons were done using unpaired t-tests with
410 Welch's correction (****: $p<0.0001$). (**d**) Representative current recordings and (**e**) current-voltage (I-V)
411 relationships of whole cell patches from TMEM16F KO HEK293T cells expressing eGFP-tagged
412 TMEM16F WT (n=6), I521K (n=5), and M522K (n=5). Currents were elicited by the voltage protocol
413 shown with the pipette solution containing 5 mM EGTA. Dotted line denotes zero current. (**f**)
414 Quantification of current at +160 mV. Currents in (**e**) and (**f**) were normalized to cell capacitance with
415 the mean ± SEM calculated from independent patches. Statistical comparisons were done using
416 unpaired t-tests with Welch's correction (*: $p<0.05$). (**g**) Lysine mutations along TM 4 in TMEM16F
417 enable spontaneous phospholipid permeation.
418

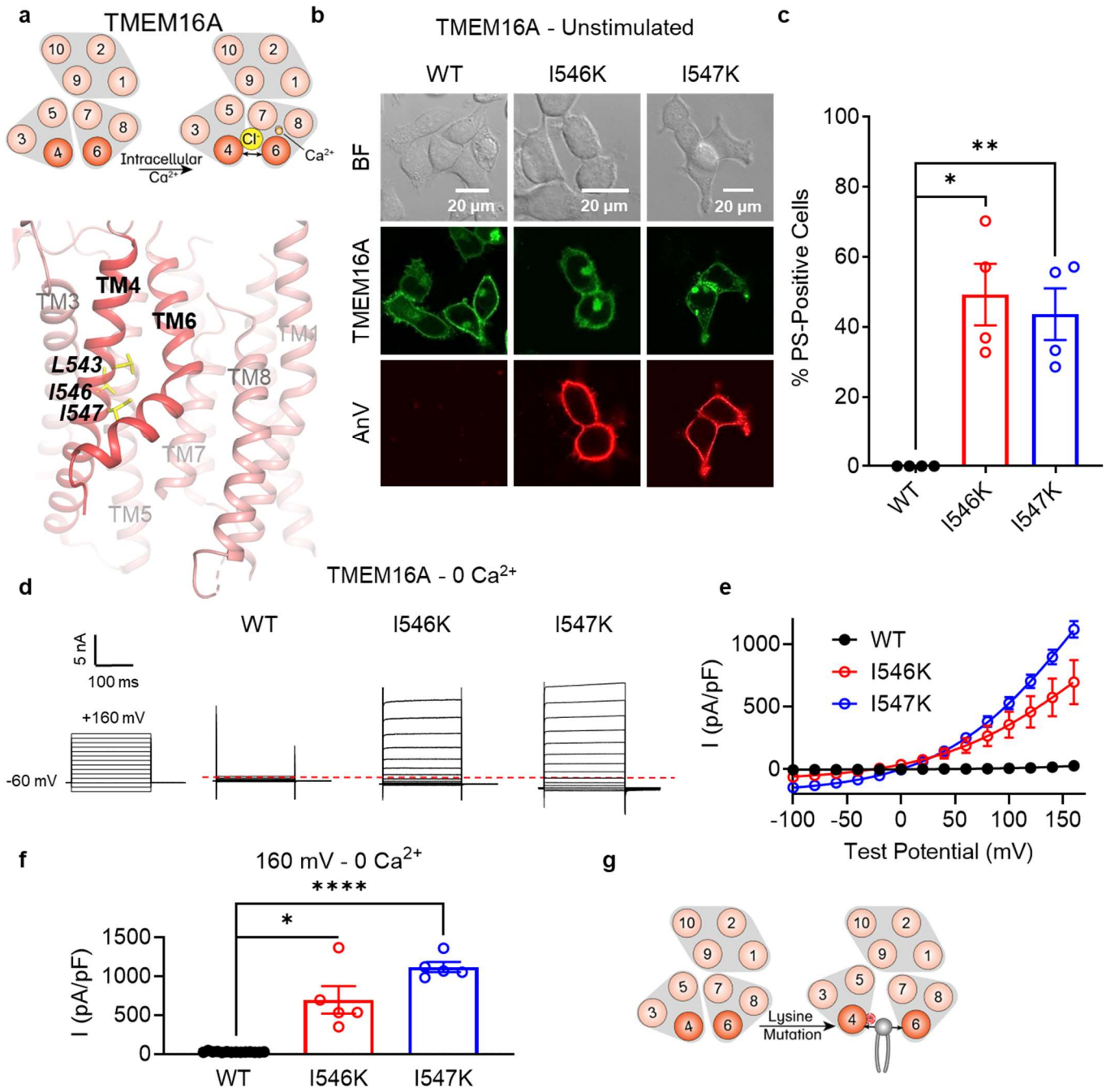

Figure 2: Lysine mutations along TM 4 enable TMEM16A channel and scramblase activities in the absence of calcium stimulation. (**a**) Top: TMEM16A is a calcium-activated chloride channel Bottom: TM 4 mutant locations mapped on TMEM16A CaCC structure (PDB 5OYG). (**b**) Representative images of TMEM16F knockout (KO) HEK293T cells expressing eGFP-tagged TMEM16A wildtype (WT), I546K, and I547K (center rows). CF 594-conjugated annexin V (AnV, bottom row) labelled PS

425 exposing cells. BF denotes bright field images (top row). (**c**) Quantification of the percentage of cells
426 with AnV labelling for TMEM16A WT (n=4), I546K (n=4), and I547K (n=4) transfected cells. Values were
427 derived from images of biological replicates, with error bars representing the standard error of the mean
428 (SEM). Statistical comparisons were done using unpaired t-tests with Welch's correction (*: $p<0.05$, **:
429 $p<0.01$). (**d**) Representative whole-cell current recordings and (**e**) current-voltage (I-V) relationships of
430 whole cell patches from TMEM16F KO HEK293T cells expressing eGFP-tagged TMEM16A WT (n=14),
431 I546K (n=5), and I547K (n=5). Currents were elicited by the voltage protocol shown with the pipette
432 containing an EGTA solution. Dotted line denotes zero current. (**f**) Quantification of current at +160 mV.
433 Currents in (**e**) and (**f**) were normalized to cell capacitance with the mean ± SEM calculated from
434 independent patches. Statistical comparisons were done using unpaired t-tests with Welch's correction
435 (*: $p<0.05$, ****: $p<0.0001$). (**g**) Lysine mutations along TM 4 in TMEM16A enable spontaneous
436 phospholipid permeation.
437

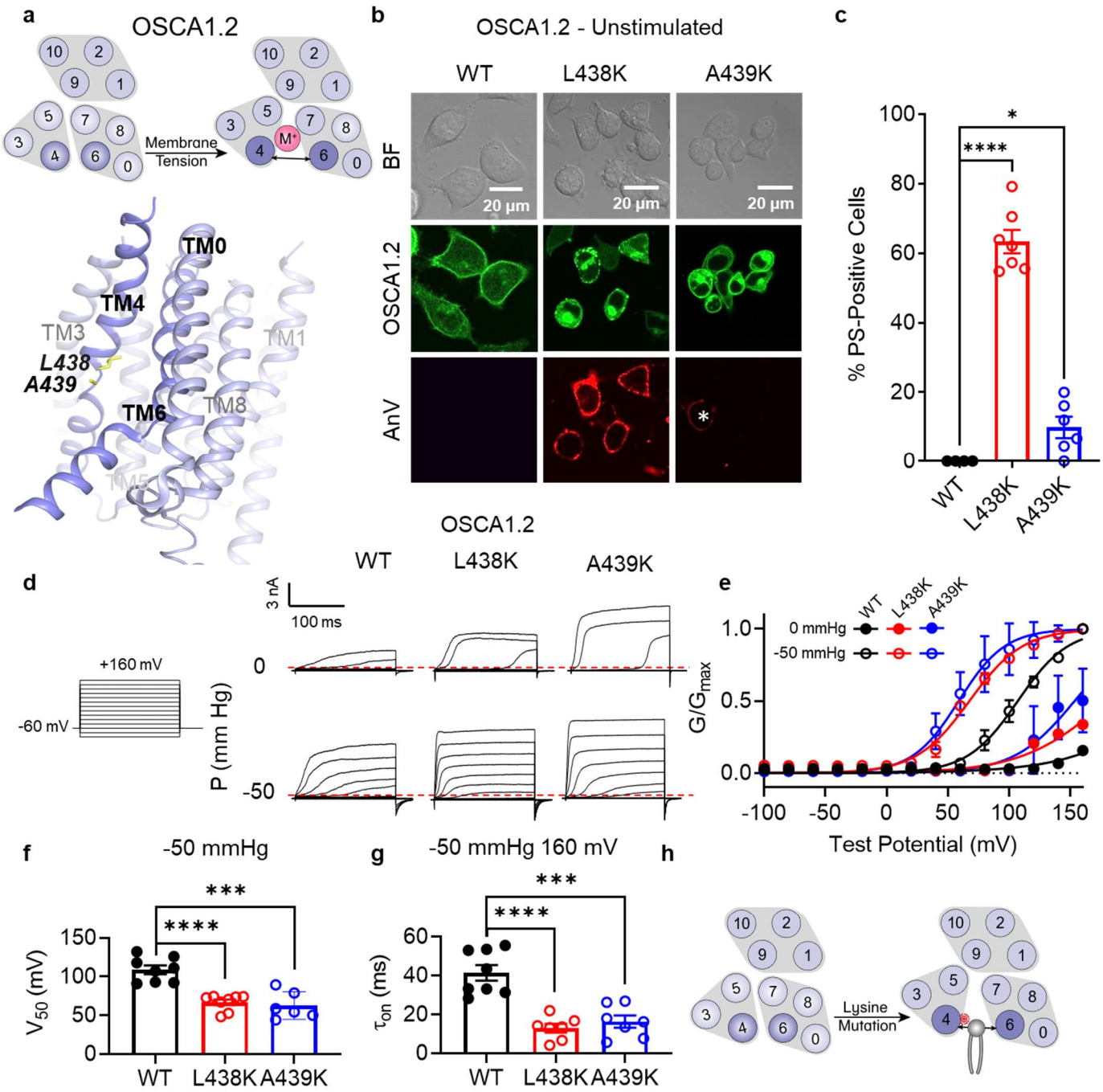

Figure 3: Lysine mutations along TM 4 enable OSCA1.2 channel and scramblase activities. Top: OSCA1.2 is a cation non-selective ion channel gated by membrane tension. Bottom: the TM 4/6 interface of OSCA1.2 (PDB 6MGV) with key residues shown as yellow sticks. (**b**) Representative images of TMEM16F KO HEK293T cells expressing eGFP-tagged (middle row) OSCA1.2 WT (left

443 column), L438K (middle column), or A439K mutants (right column). CF 594-conjugated AnV (bottom
444 row) labelled PS exposing cells. BF denotes bright field images (top row). Asterisk highlights a PS
445 positive cell for the A439K mutant. (**c**) Quantification of the percentage of cells with AnV labelling for
446 OSCA1.2 WT (n = 4), L438K (n = 7), and A439K-transfected cells (n = 6). Statistical comparisons were
447 conducted with an unpaired t-test with Welch's correction (*: $p<0.05$, ****: $p<0.0001$). (**d**) Representative
448 current recordings and (**e**) normalized conductance-voltage (*G*-*V*) relationships of inside-out patches
449 from TMEM16F KO HEK293T cells expressing eGFP-tagged OSCA1.2 WT (n=8), L438K (n=8), and
450 A439K (n = 6). Currents were elicited by the voltage protocol shown next to the listed pressures. Dotted
451 line denotes zero current. (**f**) Quantification of half-maximal voltage at -50 mmHg for WT (109 mV),
452 L438K (67 mV), and A439K (63 mV). Error bars represent standard error of the mean (SEM) calculated
453 from independent patches. Statistical comparison was conducted with an unpaired t-tests with Welch's
454 correction (***: $p<0.001$, ****: $p<0.0001$). (**g**) Quantification of activation τ_{on} at -50 mmHg and 160 mV
455 for WT (41 ms), L438K (13 ms), and A439K (16 ms). Error bars represent standard error of the mean
456 (SEM) calculated from independent patches. Statistical comparison was conducted with an unpaired t-
457 tests with Welch's correction (***: $p<0.001$, ****: $p<0.0001$). (**h**) A lysine mutation along TM 4 converts
458 OSCA1.2 channel into a phospholipid scramblase with spontaneous phospholipid permeability.
459

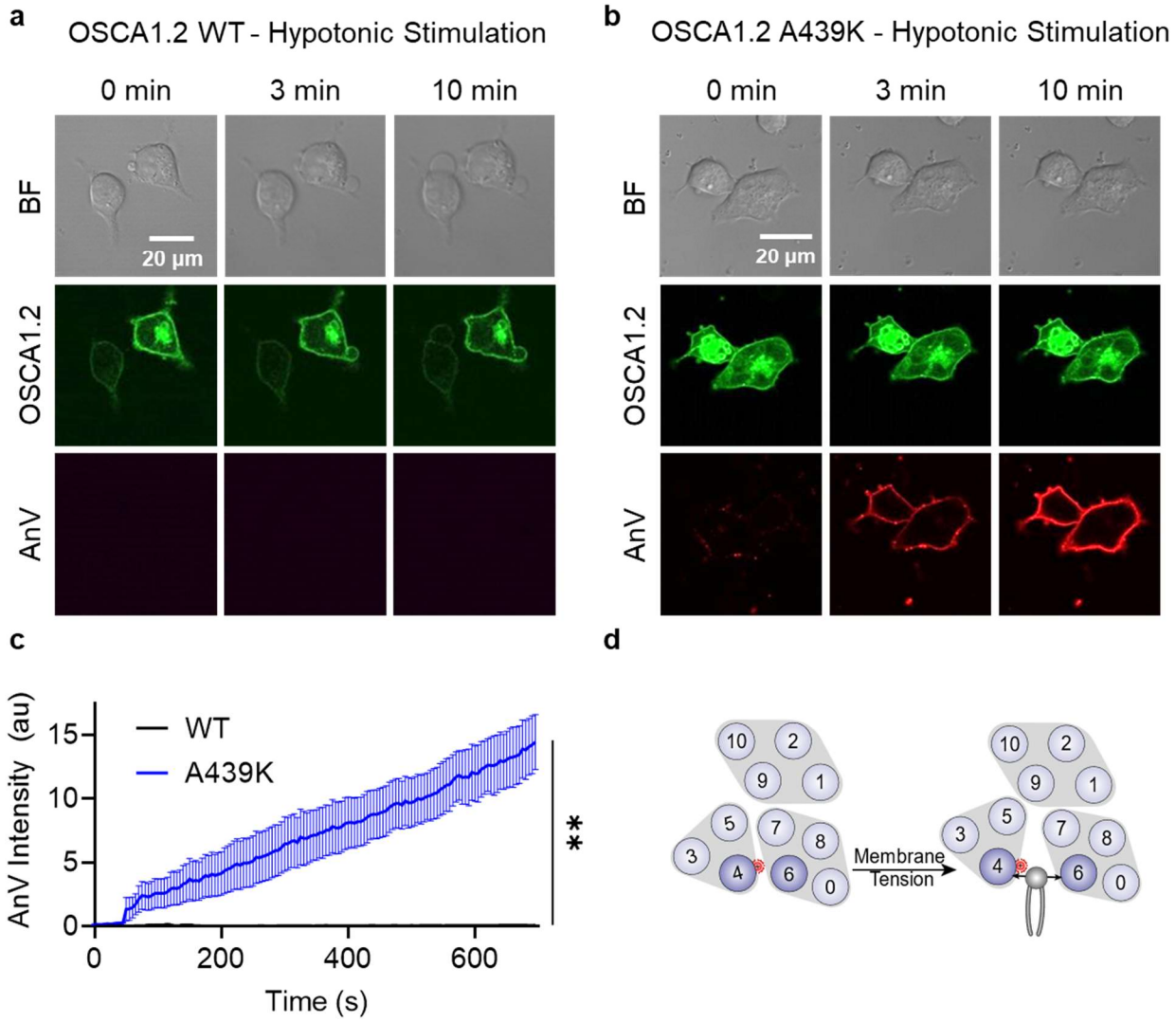

Figure 4: OSCA1.2 A439K is an osmolarity-activated scramblase.

(**a-b**) Representative images of hypotonic osmolarity stimulation of TMEM16F KO HEK293T cells expressing eGFP-tagged OSCA1.2 (**a**) WT or (**b**) the A439K mutant (center rows). CF 594-conjugated AnV (bottom rows) labelled PS exposing cells. BF denotes bright field images (top rows). Each column of representative images corresponds to the indicated time after hypo-osmotic stimulation. (**c**) Quantification of AnV intensity for OSCA1.2 WT (n=5) and A439K (n=5) after hypo-osmotic stimulation. Statistical comparison was conducted with an unpaired t-tests with Welch's correction (**: $p<0.01$). (**d**) The A439K mutation converts OSCA1.2 to an osmolarity-activated phospholipid scramblase.

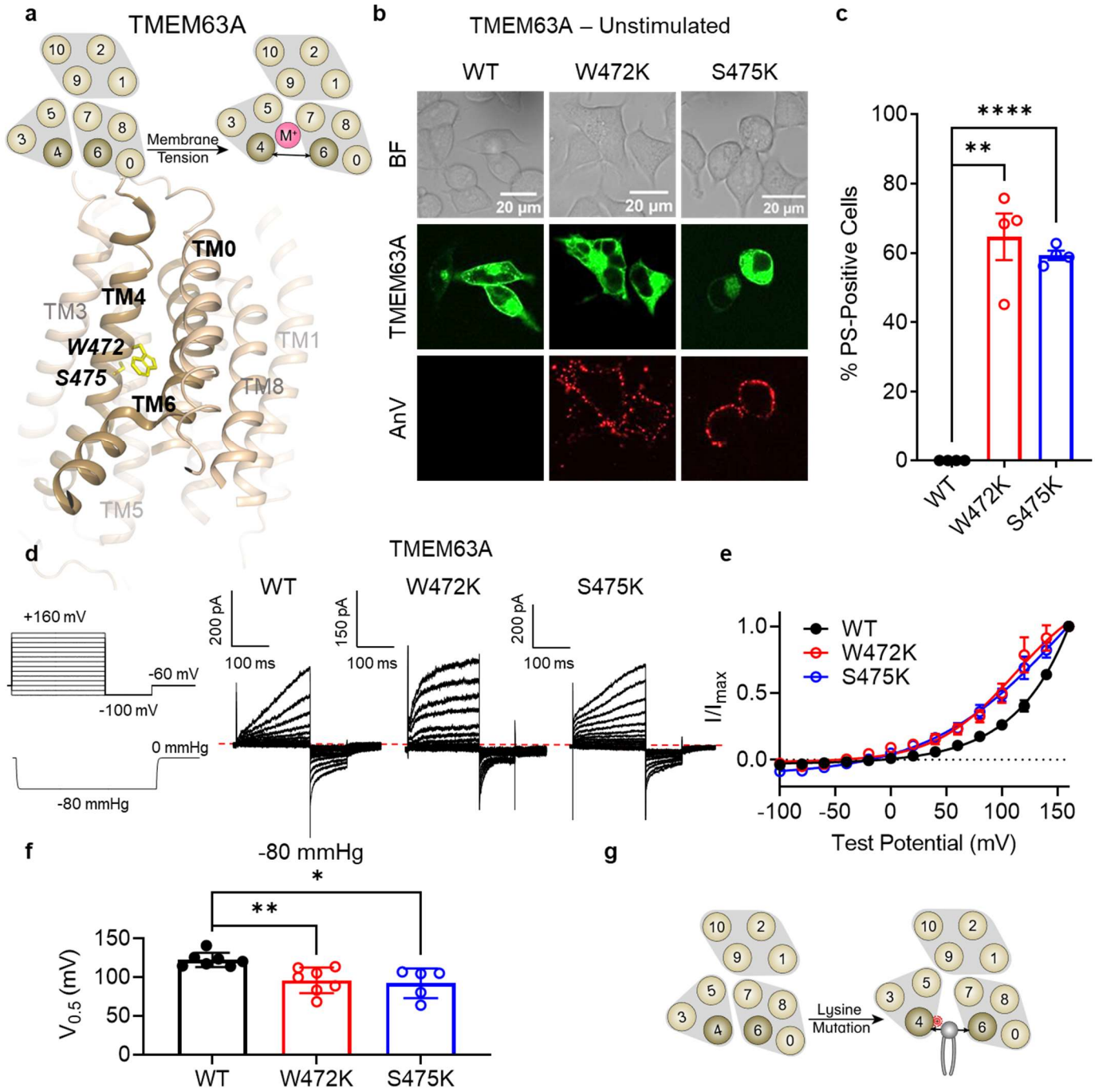

Figure 5: Lysine mutations along TM 4 enable TMEM63A channel and scramblase activities. Top: TMEM63A is a cation non-selective ion channel gated by membrane tension. Bottom: the TM 4/6 interface of *Hs*TMEM63A (PDB 8GRS) with key residues shown as yellow sticks using amino acid numbering corresponding to the mouse ortholog. (**b**) Representative images of TMEM16F KO HEK293T cells expressing eGFP-tagged (middle row) TMEM63A WT (left column), W472K (middle column), or S475K mutants (right column). CF 594-

475 conjugated AnV (bottom row) labelled PS exposing cells. BF denotes bright field images (top row). (**c**)
476 Quantification of the percentage of cells with AnV labelling for TMEM63A WT (n = 4), W472K (n = 4), and S475K-
477 transfected cells (n = 4). Statistical comparisons were conducted with unpaired t-tests with Welch's correction
478 (**: $p<0.01$, ****: $p<0.0001$). (**d**) Representative current recordings and (**e**) normalized conductance-voltage (*I-*
479 *V*) relationships of cell attached patches from TMEM16F KO HEK293T cells expressing eGFP-tagged TMEM63A
480 WT (n = 7), W472K (n = 7), and S475K (n = 5). Currents represent the subtraction of voltage alone from currents
481 elicited by the voltage and pressure protocols shown. Dotted line denotes zero current. (**f**) Quantification of half-
482 maximal voltage at -80 mmHg for WT (122 mV), W472K (96 mV), and S475K (92 mV). Error bars represent
483 standard error of the mean (SEM) calculated from independent patches. Statistical comparison was conducted
484 with an unpaired t-tests with Welch's correction (*: $p<0.05$, **: $p<0.01$). (**g**) Lysine mutations along TM 4 in
485 TMEM63A enable spontaneous phospholipid permeability.